Statistical Downscaling of Seasonal Forecast of Sea Level Anomalies for US Coasts

Xiaoyu LONG[1], Sang-Ik Shin[2], and Matthew Newman[3]

[1]University of Colorado
[2]Univ. of Colorado
[3]University of Colorado/CIRES and NOAA/PSL

November 22, 2022

Abstract

Increasing coastal inundation risk in a warming climate will require accurate and reliable seasonal forecasts of sea level anomalies at fine spatial scale. In this study, we explore statistical downscaling of monthly hindcasts from six current seasonal prediction systems to provide high resolution prediction of sea level anomalies along the North American coast, including at several tide gauge stations. This involves applying a seasonally-invariant downscaling operator, constructing by linearly regressing high-resolution ($1/12^{\circ}$) ocean reanalysis data against its coarse-grained (1°) counterpart, to each hindcast ensemble member for the period 1982-2011. The resulting high resolution coastal hindcasts are significantly more skillful than the original hindcasts interpolated onto the high resolution grid. Most of this improvement occurs during summer and fall, without impacting the seasonality of skill noted in previous studies. Analysis of the downscaling operator reveals that it boosts skill by amplifying the most predictable pattern while damping the less predictable pattern.

Statistical Downscaling of Seasonal Forecast of Sea Level Anomalies for US Coasts

Xiaoyu Long[1,2], **Sang-Ik Shin**[1,2] **and Matthew Newman**[1,2]

[1]CIRES, University of Colorado Boulder, Boulder, CO, USA
[2]NOAA Physical Sciences Laboratory, Boulder, CO, USA

Key Points:

- Sea level prediction from relatively coarse operational forecasts can be enhanced to finer coastal scales using statistical downscaling
- Downscaling can be determined by multivariate linear regression trained from high-resolution reanalysis and its coarse-grained counterpart
- This downscaling method significantly improves skill compared to bilinearly interpolated hindcasts at several US tide gauge locations

Abstract

Increasing coastal inundation risk in a warming climate will require accurate and reliable seasonal forecasts of sea level anomalies at fine spatial scale. In this study, we explore statistical downscaling of monthly hindcasts from six current seasonal prediction systems to provide high resolution prediction of sea level anomalies along the North American coast, including at several tide gauge stations. This involves applying a seasonally-invariant downscaling operator, constructing by linearly regressing high-resolution ($1/12^{\circ}$) ocean reanalysis data against its coarse-grained (1°) counterpart, to each hindcast ensemble member for the period 1982-2011. The resulting high resolution coastal hindcasts are significantly more skillful than the original hindcasts interpolated onto the high resolution grid. Most of this improvement occurs during summer and fall, without impacting the seasonality of skill noted in previous studies. Analysis of the downscaling operator reveals that it boosts skill by amplifying the most predictable pattern while damping the less predictable pattern.

Plain Language Summary

The typical resolution of current seasonal climate forecast systems is too coarse to meet the needs for coastal ocean management and services including sea level forecast along U.S. coasts. This is becoming an increasingly important need as sea levels rise in a warming climate. To provide such information, we developed an efficient way to make predictions of sea level on much smaller spatial scales, on the order of 10 km. We tested our approach by using past forecasts ("hindcasts") from existing climate forecast systems using the observed statistical relationship between sea level variations on scales of 100-1000 km and finer-scale coastal ocean observations. Our statistical approach improves the hindcast skill by which it projects and amplifies some of the predictable large basin-scale signals to coastal ocean fine structures.

1 Introduction

Sea level rise has increased the frequency, severity, and duration of coastal flooding in the past few decades (Sweet et al., 2014; Wdowinski et al., 2016; Ezer & Atkinson, 2014; Moftakhari et al., 2015). These changes can impact coastal communities through groundwater inundation (Rotzoll & Fletcher, 2013), beach erosion (Anderson et al., 2015) and storm-drain backflow and damage to the infrastructure (Habel et al., 2020). Coastal flooding frequency, due both to accelerated sea level rise (Sallenger et al., 2012; Nerem et al., 2018) and increasing sea level variability under climate change (Widlansky et al., 2020), is projected to steadily increase (Dahl et al., 2017; Kruel, 2016; Kriebel et al., 2015; Thompson et al., 2021; Wdowinski et al., 2016) and double by 2050 (Vitousek et al., 2017). This increasing risk to coastal infrastructure necessitates more accurate and reliable prediction of high-water level events months and seasons in advance.

Previous studies have demonstrated that dynamical seasonal forecasting systems can forecast sea level variation in the open ocean and at some coastal locations (Miles et al., 2014; McIntosh et al., 2015; Widlansky et al., 2017; Long et al., 2021), but in general prediction for coastal regions remains challenging. First, by definition the coasts are the numerical boundary of the ocean model and require special treatment in the numerical integration. Second, the spatial resolution of the current generation of forecast systems is too coarse to fully resolve the topography and fine-scale dynamics near the coasts. This issue could be addressed by employing much finer grid spacing in the global forecast models, but the resulting computational burden and model output storage requirements would be considerable, especially given the need for multiple ensemble members.

Alternatively, through the use of downscaling techniques (Pielke Sr & Wilby, 2012; Castro et al., 2005), regional forecast output with higher resolution than that of the original coarse-grained forecast system can be obtained either dynamically, using regional numerical models with higher resolution but in a limited domain, or statistically, by finding a statistical relationship between coarse-grained and fine-scale data. Dynamical downscaling can potentially benefit from the resolved dynamics (other than parameterized processes) and topography in the regional model compared to coupled GCMs (M. A. Alexander et al., 2020; Shin & Alexander, 2020). Yet, it still requires substantial computational and storage resources. Statistical downscaling, on the other hand, usually provide comparable results without the need for lengthy numerical integration and is often used as a benchmark against which dynamic downscaling is evaluated (Goubanova et al., 2011).

This study aims to develop a high resolution forecast of coastal sea level anomalies from the existing seasonal forecast product using a simple regression-based statistical downscaling method, whose results can serve as a benchmark for evaluation of future development of more advanced statistical and dynamical downscaling methods. This paper is organized as follows. Section 2 introduces the observational and reanalysis data and model hindcast dataset used in this study. Section 3 describes the details of the regression-based downscaling procedure. The validation of the downscaling technique and the skill of the downscaled hindcasts are presented in Section 4. Section 5 includes the conclusion.

2 Data description

To assess the skill of the statistical downscaling, we use monthly observations of sea level from coastal tide gauges, sea surface height (SSH) fields from reanalysis and coupled climate model hindcast products.

2.1 Tide Gauge Observation

Six tide gauge stations (black dots in Fig. 1: San Diego, San Francisco, South Beach, Virginia Key, Charleston and Atlantic City) are chosen to represent typical coastal locations in the United States. Tide gauge observations usually have long time coverage and are fairly consistent with other observations such as Satellite Altimetry (Long et al., 2021).

2.2 GLORYS Reanalysis

GLORYS Ocean Reanalysis Version 12v1 (hereafter GLORYS; Jean-Michel et al., 2021, and references therein) is a global eddy-resolving ocean and sea ice reanalysis, carried out by the Copernicus Marine Environment Monitoring Service (CMEMS), which provides monthly ocean fields in $1/12°$ horizontal resolution and 50 vertical levels, and covers the period from 1993 to present. The reanalysis system assimilates along-track satellite derived sea level anomalies, satellite derived sea surface temperature, and in situ temperature and salinity vertical profiles , but not tide gauge data. However, extensive comparison shows that the SSH output from GLORYS is highly correlated with tide gauge observation along the U.S. coastlines (Amaya et al., 2022, and Fig. S1).

2.3 Hindcasts

We downscaled hindcasts from six current generation seasonal forecast systems (Table S1), developed by different operational centers around the world, using models with different resolution, assimilation and parameterization schemes (Merryfield et al., 2013; Kirtman et al., 2014; Saha et al., 2014; Zhang et al., 2007). Hindcast ensembles of SSH from each of these models, initialized at each calendar month from 1982 to 2011 with lead time up to 12 months, were used in this study. We defined the lead-1 month as the same month during which the model forecast is initialized. For example, if the forecast was initialized on January 1st, then the monthly averaged forecast for January was the lead-1 month forecast (other studies might call it lead-0 or lead-0.5 month), February is the lead-2 month forecast, and so on. To remove the mean bias (model drift) in the hindcasts, we removed the initial time and lead-time dependent climatology determined separately for each model, which is a common practice for seasonal forecasts that are initialized with full field variables (Smith et al., 2013; Vannitsem et al., 2018).

3 Statistical Downscaling

We explore determining the downscaling relationship by relating an observational fine-scale dataset to a coarse-grained version of itself. The resulting relationship, when applied to the bias-corrected hindcasts, then yields downscaled hindcasts. In such practices, it is common that the predictor domain is different from the predictand domain (Goubanova et al., 2011), and the former is usually larger than the latter to capture the large scale variations. We set the predictor as the coarse-grained SSH anomalies determined by regridding the GLORYS reanalysis onto the climate model hindcast resolution ($1^\circ \times 1^\circ$) using an areal conservative method, so that the downscaling operator derived from the observational datasets can be directly used to downscale the coupled model hindcasts. The predictand is set as the SSH anomalies from the GLORYS reanalysis on its original grid. Here, the anomalies were defined as departures from the monthly climatology for the years 1993-2018.

3.1 Domain for Predictor and Predictand

To identify a relevant geographic domain for the predictor, the coarse-grained SSH anomalies were regressed onto each of the tide gauge observed sea level anomalies (Fig. 1). For the West Coast (Fig. 1a, b and c), coastal sea level variability is tightly confined to a narrow region along the coastline, dominated by coastally-trapped Kelvin Waves (Allen, 1975) whose source can be traced back to the Tropics (Meyers et al., 1998). The sea level variability at San Diego (Fig. 1a) is associated more strongly with coastal SSH signals and less with the open basin SSH pattern, as opposed to farther up the coast in South Beach (Fig. 1c) where the situation is reversed. Hence, to capture the large-scale pattern associated with coastal variability for all three representative tide gauges, the predictor domain for the West Coast was chosen be all ocean points between 20N to 70N and 150W to 110W.

The dynamics of coastal variability for the East Coast are different from those of the West Coast. Along the southeast US coast (Fig. 1d and e), sea level variability is associated with the western boundary current (i.e., the Gulf Stream) and its extension. The weakly positive regression along the Gulf of Mexico indicates that part of the signal is from coastally-trapped waves propagating from the southeast US coast to the Gulf of Mexico (Pasquet et al., 2013; Ezer, 2016). In contrast, sea level variability near the northeast coast (Fig. 1f) appears mostly influenced by local processes. The predictor domain for the East Coast was therefore bounded between 20N to 50N and 90W to 60W.

The West Coast predictand domain was set to be the area within 200km of the coastline and within the larger predictor domain, while for the East Coast we adopt the Southeast and Northeast US Continental Shelf Large Marine Ecosystem regions (L. M. Alexander, 1993). We have tested different reasonable choices for the predictor and predictand domains, and our results are not sensitive to these choices.

3.2 Downscaling procedure

The key element of statistical downscaling is to find a statistical relationship between the predictors and the predictands of interest (e.g. Goubanova et al., 2011, and many references therein). A multiple linear regression (MLR) in EOF space was used to determined the statistical relationship between the coarse-grained and fine-scale SSH anomalies. The SSH anomalies were further truncated via EOF analysis to minimize the sampling uncertainty and thus reduce the effective degree of freedom (i.e. dimensionality) of limited observation records. Here we used predictor/predictand truncation of 34 /10 EOFs for the West Coast, and 40/5 EOFs for the East Coast, respectively. Those truncation was chosen via extensive 10-fold cross-validation, where 90% of the data was used to determine the operator, which was then used to downscale the remaining 10%; this process was cycled through ten times, for each possible permutation of predictor/predictand truncation pairs (see details in Supplementary Text S1 and Fig. S2).

Then, the downscaling procedure via MLR becomes:

$$\mathbf{y} = \mathbf{B}\mathbf{x} + \epsilon \tag{1}$$

where $\mathbf{x}$ and $\mathbf{y}$ are vectors representing the principal component (PC) time series of predictor and predictand, respectively, $\mathbf{B}$ is the multivariate regression coefficient (i.e. downscaling operator) matrix and ϵ is the regression error. In order to account for spatial heterogeneity, the MLR is performed between two spatially varying fields, so that $\mathbf{B}$ has nonzero off-diagonal elements. Moreover, EOF truncations for the predictor and predictand are different, so $\mathbf{B}$ need not be square. Once the regression coefficient matrix $\mathbf{B}$ is determined by minimizing the cross-validated regression error, we use it to downscale the hindcast in geographical space (Ym):

$$\mathbf{Y_m} = \Phi\mathbf{B}\Psi^{\intercal}\mathbf{X_m}$$

where Φ and Ψ are the empirical orthogonal functions corresponding to the PC time series in $\mathbf{y}$ and $\mathbf{x}$ respectively.

3.3 Testing downscaling against interpolation

The statistical downscaling approach infers the forecast on a fine-scale grid from the forecast on a coarse grid by relating observed large-scale variations to fine-scale variations. We hypothesize that this approach is superior to instead filling in the fine grid using an interpolation technique, which uses information from the nearby grid points alone, but not from the large-scale patterns. In order to justify the statistical downscaling, we compared our downscaled hindcasts with a simple extrapolation/interpolation method to delineate local (interpolation via nearby coastal points) versus remote (basin to coastal scale) influences. To this end, we created an interpolated hindcast dataset: we fill the grid points on continents (i.e. extrapolation) by solving a Poisson's equation on a coarse $1^\circ \times 1^\circ$ grid, and then use bilinear interpolation to find the values on the GLORYS ocean grid.

4 Results

4.1 Regression Validation

We first show how well the downscaling operators can reproduce the observed finescale coastal SSH anomalies. Figure 2 shows that the downscaled SSH anomalies are generally highly accurate within the West Coast domain (Fig. 2a), with the correlation between the downscaled SSH anomalies and the original GLORYS data above 0.9 for most locations. These correlations are reduced away from the coast, especially around 40N, regions with strong mesoscale eddy activity (Stammer, 1997) where our multivariate linear regression technique might have difficulty capturing the relationship between coarse-grained and fine-scale variability. Downscaled SSH anomalies are also highly correlated with GLORYS in the East Coast domain (Fig. 2b). However, the correlation is higher along the Southeast than the Northeast continental shelf, suggesting that the sea level variability in the former is associated with large scale SSH variations while the latter is more influenced by local processes, which is also consistent with the regression maps in Fig. 1. Overall, the linear regression captured the relationship between the coarse-grained and fine-scale SSH anomalies with reasonable accuracy for both coastal regions, despite their differing dynamics.

4.2 Forecast Skill

The patterns of skill of both downscaled and interpolated multi-model ensemble mean hindcasts are generally similar (Fig. 3a and b). For the West Coast, the highest skill is realized along the southwest coast, which could be attributed to coastally-trapped Kelvin Waves. Low skill is found in the offshore region around 40N and in the Gulf of Alaska. Downscaling generally improved upon interpolated forecast skill, significantly so along the midlatitude coasts and in the Gulf of Alaska region (Fig. 3c). The SVD analysis of the downscaling operator (Fig. S6) shows that this improvement is primarily due to one single-signed coarse-grained pattern along the coast that is amplified by the downscaling. For the East Coast, where overall skill is notably lower than for the West Coast, downscaling still improved skill in a few areas, notably along the Northeast continental shelf and in a Southeast continental shelf region away from the coastline. Again, much of this improvement is dominated by one single-signed coastal pattern (Fig. S7). The effectiveness of the statistical downscaling method varies across the models (Fig. S7 to S12), with much more downscaling improvement for the CanCM3 and CanCM4 than the other models.

Figure 4 shows the skill of hindcasts verified against tide gauge observations. Since tide gauge data are not assimilated into GLORYS, they provide an independent verification of our technique. For San Diego and San Francisco, statistically downscaled hindcasts had significantly improved skill compared to interpolated hindcasts for almost all lead times. There is no significant difference in the skill between downscaling and interpolation for South Beach except at lead-1 month. For the three stations on the East Coast (Fig. 4d, e and f), downscaled forecasts are significantly more skillful than interpolated forecasts for most lead times.

SSH forecast skill has strong seasonality (Long et al., 2021) that is typically a function of the verification month (Shin & Newman, 2021). Figure 5 show the skill for each target month and lead time for San Diego and Charleston (other stations are shown in Fig. S4). San Diego has higher skill for hindcasts verifying during the cold season than for those verifying during the warm season, particularly for October through February, consistent with a predictable signal due to ENSO-forced coastally-trapped Kelvin Waves (Amaya et al., 2022). West coast sea level variability is also smaller in warm than in cold months. The skill of interpolated forecasts has similar seasonality. However, the seasonality of the skill is different than that of the skill difference. For example, statistical downscaling improves San Diego hindcast skill during both October-December and April-June. San Francisco and South Beach show similar seasonality of skill and skill difference as San Diego. In contrast, higher skill for the east coast stations is found for hindcasts verifying during late summer and early autumn, for both downscaling and interpolation, which is also when the most significant downscaling skill improvement is found (Fig. 5 and S2). It is also interesting that the downscaling leads to minimal skill improvement, or even a minor degradation of skill, during some winter months for most of the stations examined here.

5 Conclusion

In this study, we demonstrated a statistical downscaling procedure for the seasonal forecast of SSH anomalies for US coasts. The downscaling operator obtained by regressing fine-scale SSH anomalies onto coarse-grained SSH anomalies can be applied to model forecasts to generate a high resolution product. We showed that our statistical downscaling technique can implicitly retrieve some of the skill existing in the fine-scale variation. This skill improvement would not have been obtained if we had only interpolated the model output to a fine-scale grid, because the fine-scale variabilty is not resolved in the coarse-grained model grid. Indeed, this downscaling technique significantly improved the hindcast skill of SSH anomalies for the US coasts compared to bilinearly interpolated hindcasts. When comparing the downscaled hindcast to the selected six tide gauge observations, we found that the downscaled hindcast improved skill for five stations at most lead times. While the downscaling did not alter the seasonality of the skill, the skill improvement has different seasonality, for reasons that remain to be explained. One possibility is that the downscaling was assumed to be independent of the seasonal cycle, so potential improvement might be expected if seasonal variation in the statistical relationship is included.

In this study, we have not aimed to "correct" the hindcasts for model error, apart from removing the mean bias. That is, when the reanalysis-derived downscaling operator is applied to the model hindcasts it is assumed that the model space is largely similar to that of the reanalysis. Of course, in reality these models generate different variability than observations or reanalysis, and their hindcasts may evolve in a different state space than nature (e.g., Ding et al., 2018), which may be why some model hindcasts are more improved than others by the downscaling. Applying a downscaling relationship determined entirely from observations to coarse-grained forecasts might therefore provide less high resolution skill than a downscaling trained on the forecasts themselves, which provides a focus for future work.

Data Availability Statement

The data used in this study are available from the following sources: tide gauge observations (`https://psl.noaa.gov/data/tidal/`), GLORYS reanalysis (`https://datastore.cls.fr/catalogues/eu-copernicus-marine-service-global-reanalysis-glorys/`) and retrospective forecasts (`https://downloads.psl.noaa.gov/Projects/NMME/`).

Acknowledgments
We thank Dr. Michael Alexander and Dr. Antonietta Capotondi for their constructive suggestion. We also thank the modeling centers for providing the seasonal forecast output.

References

Alexander, L. M. (1993). Large marine ecosystems: A new focus for marine resources management. *Marine Policy*, *17*(3), 186–198.

Alexander, M. A., Shin, S.-i., Scott, J. D., Curchitser, E., & Stock, C. (2020). The response of the northwest atlantic ocean to climate change. *Journal of Climate*, *33*(2), 405–428.

Allen, J. (1975). Coastal trapped waves in a stratified ocean. *Journal of Physical Oceanography*, *5*(2), 300–325.

Amaya, D. J., Jacox, M. G., Dias, J., Alexander, M. A., Karnauskas, K. B., Scott, J. D., & Gehne, M. (2022). Subseasonal-to-seasonal forecast skill in the california current system and its connection to coastal kelvin waves. *Journal of Geophysical Research: Oceans*, *127*(1), e2021JC017892. Retrieved from `https://agupubs.onlinelibrary.wiley.com/doi/abs/10.1029/2021JC017892` (e2021JC017892 2021JC017892) doi: https://doi.org/10.1029/2021JC017892

Anderson, T. R., Fletcher, C. H., Barbee, M. M., Frazer, L. N., & Romine, B. M.

(2015). Doubling of coastal erosion under rising sea level by mid-century in hawaii. *Natural Hazards*, *78*(1), 75–103.

Castro, C. L., Pielke Sr, R. A., & Leoncini, G. (2005). Dynamical downscaling: Assessment of value retained and added using the regional atmospheric modeling system (rams). *Journal of Geophysical Research: Atmospheres*, *110*(D5).

Dahl, K. A., Fitzpatrick, M. F., & Spanger-Siegfried, E. (2017). Sea level rise drives increased tidal flooding frequency at tide gauges along the us east and gulf coasts: Projections for 2030 and 2045. *PloS one*, *12*(2), e0170949.

Ding, H., Newman, M., Alexander, M. A., & Wittenberg, A. T. (2018). Skillful climate forecasts of the tropical indo-pacific ocean using model-analogs. *Journal of Climate*, *31*(14), 5437–5459.

Ezer, T. (2016). Can the gulf stream induce coherent short-term fluctuations in sea level along the us east coast? a modeling study. *Ocean Dynamics*, *66*(2), 207–220.

Ezer, T., & Atkinson, L. P. (2014). Accelerated flooding along the us east coast: On the impact of sea-level rise, tides, storms, the gulf stream, and the north atlantic oscillations. *Earth's Future*, *2*(8), 362–382.

Goubanova, K., Echevin, V., Dewitte, B., Codron, F., Takahashi, K., Terray, P., & Vrac, M. (2011). Statistical downscaling of sea-surface wind over the peru–chile upwelling region: diagnosing the impact of climate change from the ipsl-cm4 model. *Climate Dynamics*, *36*(7), 1365–1378.

Habel, S., Fletcher, C. H., Anderson, T. R., & Thompson, P. R. (2020). Sea-level rise induced multi-mechanism flooding and contribution to urban infrastructure failure. *Scientific reports*, *10*(1), 1–12.

Jean-Michel, L., Eric, G., Romain, B.-B., Gilles, G., Angélique, M., Marie, D., ... others (2021). The copernicus global 1/12° oceanic and sea ice glorys12 reanalysis. *Frontiers in Earth Science*, *9*, 585.

Kirtman, B. P., Min, D., Infanti, J. M., Kinter, J. L., Paolino, D. A., Zhang, Q., ... Wood, E. F. (2014, April). The North American Multimodel Ensemble: Phase-1 seasonal-to-interannual prediction; phase-2 toward developing intraseasonal prediction. *Bulletin of the American Meteorological Society*, *95*(4), 585–601. doi: 10.1175/BAMS-D-12-00050.1

Kriebel, D. L., Geiman, J. D., & Henderson, G. R. (2015). Future flood frequency under sea-level rise scenarios. *Journal of Coastal Research*, *31*(5), 1078–1083.

Kruel, S. (2016). The impacts of sea-level rise on tidal flooding in boston, massachusetts. *Journal of Coastal Research*, *32*(6), 1302–1309.

Long, X., Widlansky, M. J., Spillman, C. M., Kumar, A., Balmaseda, M., Thompson, P. R., ... Mitchum, G. (2021). Seasonal forecasting skill of sea-level anomalies in a multi-model prediction framework. *Journal of Geophysical Research: Oceans*, *126*(6), e2020JC017060. Retrieved from `https://agupubs.onlinelibrary.wiley.com/doi/abs/10.1029/2020JC017060` (e2020JC017060 2020JC017060) doi: https://doi.org/10.1029/2020JC017060

McIntosh, P. C., Church, J. A., Miles, E. R., Ridgway, K., & Spillman, C. M. (2015). Seasonal coastal sea level prediction using a dynamical model. *Geophysical Research Letters*, *42*(16), 6747–6753.

Merryfield, W. J., Lee, W.-S., Boer, G. J., Kharin, V. V., Scinocca, J. F., Flato, G. M., ... Polavarapu, S. (2013). The canadian seasonal to interannual prediction system. part i: Models and initialization. *Monthly weather review*, *141*(8), 2910–2945.

Meyers, S. D., Melsom, A., Mitchum, G. T., & O'Brien, J. J. (1998). Detection of the fast kelvin wave teleconnection due to el niño-southern oscillation. *Journal of Geophysical Research: Oceans*, *103*(C12), 27655–27663.

Miles, E. R., Spillman, C. M., Church, J. A., & McIntosh, P. C. (2014). Seasonal prediction of global sea level anomalies using an ocean–atmosphere dynamical model. *Climate dynamics*, *43*(7), 2131–2145.

Moftakhari, H. R., AghaKouchak, A., Sanders, B. F., Feldman, D. L., Sweet, W., Matthew, R. A., & Luke, A. (2015). Increased nuisance flooding along the coasts of the united states due to sea level rise: Past and future. *Geophysical Research Letters*, *42*(22), 9846–9852.

Nerem, R. S., Beckley, B. D., Fasullo, J. T., Hamlington, B. D., Masters, D., & Mitchum, G. T. (2018). Climate-change–driven accelerated sea-level rise detected in the altimeter era. *Proceedings of the national academy of sciences*, *115*(9), 2022–2025.

Pasquet, S., Vilibić, I., & Šepić, J. (2013). A survey of strong high-frequency sea level oscillations along the us east coast between 2006 and 2011. *Natural Hazards and Earth System Sciences*, *13*(2), 473–482.

Pielke Sr, R. A., & Wilby, R. L. (2012). Regional climate downscaling: What's the point? *Eos, Transactions American Geophysical Union*, *93*(5), 52–53.

Rotzoll, K., & Fletcher, C. H. (2013). Assessment of groundwater inundation as a consequence of sea-level rise. *Nature Climate Change*, *3*(5), 477–481.

Saha, S., Moorthi, S., Wu, X., Wang, J., Nadiga, S., Tripp, P., ... others (2014). The ncep climate forecast system version 2. *Journal of climate*, *27*(6), 2185–2208.

Sallenger, A. H., Doran, K. S., & Howd, P. A. (2012). Hotspot of accelerated sea-level rise on the atlantic coast of north america. *Nature Climate Change*, *2*(12), 884–888.

Shin, S.-I., & Alexander, M. A. (2020). Dynamical downscaling of future hydrographic changes over the northwest atlantic ocean. *Journal of Climate*, *33*(7), 2871–2890.

Shin, S.-I., & Newman, M. (2021). Seasonal predictability of global and north american coastal sea surface temperature and height anomalies. *Geophysical Research Letters*, *48*(10), e2020GL091886.

Smith, D. M., Eade, R., & Pohlmann, H. (2013). A comparison of full-field and anomaly initialization for seasonal to decadal climate prediction. *Climate Dynamics*, *41*(11), 3325–3338.

Stammer, D. (1997). Global characteristics of ocean variability estimated from regional topex/poseidon altimeter measurements. *Journal of Physical Oceanography*, *27*(8), 1743–1769.

Sweet, W., Park, J., Marra, J., Zervas, C., & Gill, S. (2014). *Sea level rise and nuisance flood frequency changes around the united states* (Tech. Rep.). Silver Spring, Maryland, United States: NOAA technical report NOS CO-OPS 073.

Thompson, P. R., Widlansky, M. J., Hamlington, B. D., Merrifield, M. A., Marra, J. J., Mitchum, G. T., & Sweet, W. (2021). Rapid increases and extreme months in projections of united states high-tide flooding. *Nature Climate Change*, *11*(7), 584–590.

Vannitsem, S., Wilks, D. S., & Messner, J. (2018). *Statistical postprocessing of ensemble forecasts.* Elsevier.

Vitousek, S., Barnard, P. L., Fletcher, C. H., Frazer, N., Erikson, L., & Storlazzi, C. D. (2017). Doubling of coastal flooding frequency within decades due to sea-level rise. *Scientific reports*, *7*(1), 1–9.

Wdowinski, S., Bray, R., Kirtman, B. P., & Wu, Z. (2016). Increasing flooding hazard in coastal communities due to rising sea level: Case study of miami beach, florida. *Ocean & Coastal Management*, *126*, 1–8.

Widlansky, M. J., Long, X., & Schloesser, F. (2020). Increase in sea level variability with ocean warming associated with the nonlinear thermal expansion of seawater. *Communications Earth & Environment*, *1*(1), 1–12.

Widlansky, M. J., Marra, J. J., Chowdhury, M. R., Stephens, S. A., Miles, E. R., Fauchereau, N., ... Wells, J. (2017). Multimodel ensemble sea level forecasts for tropical pacific islands. *Journal of Applied Meteorology and Climatology*, *56*(4), 849–862.

Zhang, S., Harrison, M., Rosati, A., & Wittenberg, A. (2007). System design and evaluation of coupled ensemble data assimilation for global oceanic climate studies. *Monthly Weather Review*, *135*(10), 3541–3564.

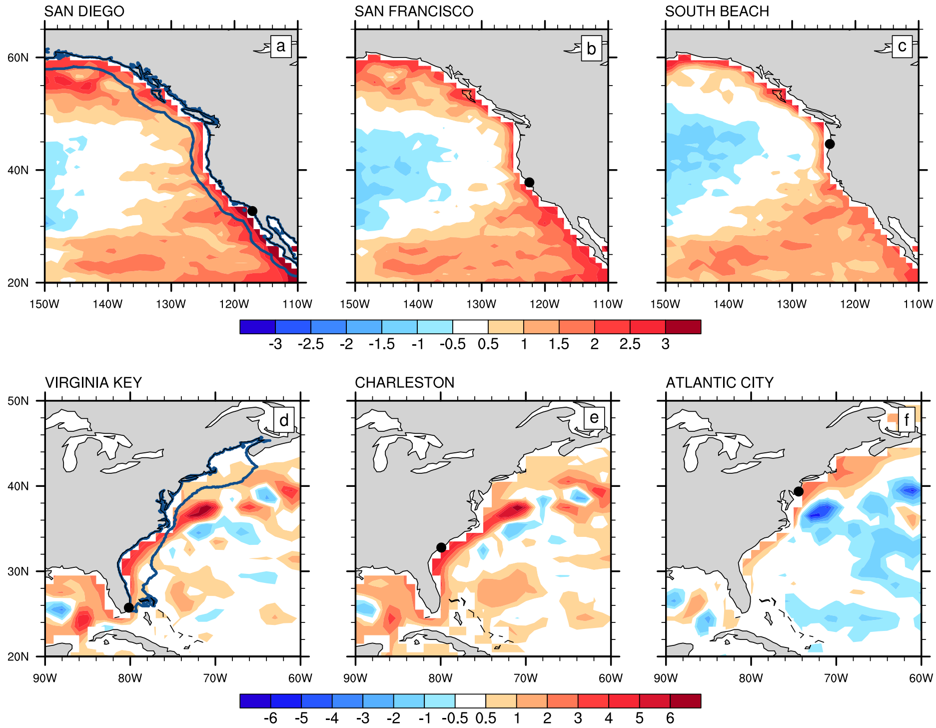

Figure 1. Regression maps of SSH anomalies from coarsened GLORYS reanalysis (1x1 grid spacing) onto each tide gauge observed sea level anomalies. The unit is centimeter. The name of each tide gauge is shown on the top of each panel. The black dots indicate the locations of the tide gauges. The blue line in panel (a) and (d) indicate the domain used in the MLR for predictand.

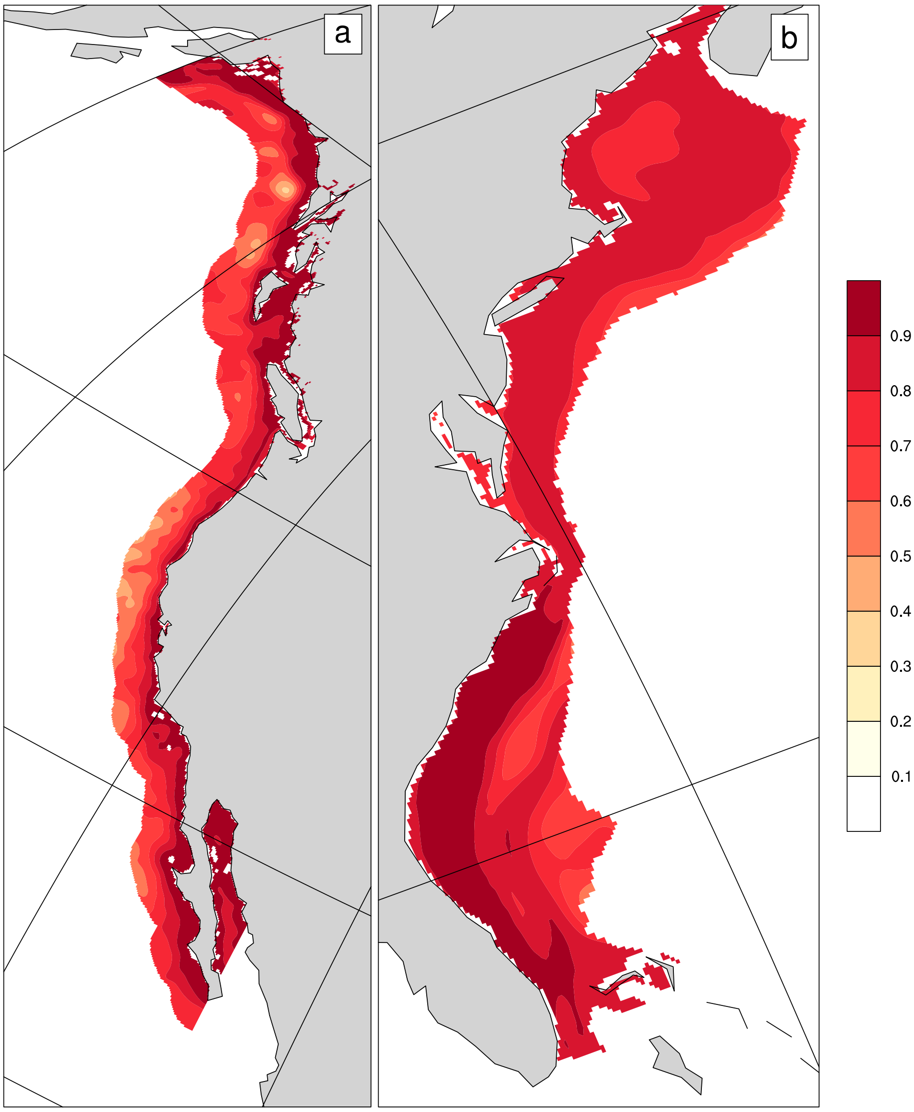

Figure 2. Temporal correlation coefficient between the SSH anomalies from GLORYS and the regression predicted SSH anomalies for (a) West Coast and (b) East Coast.

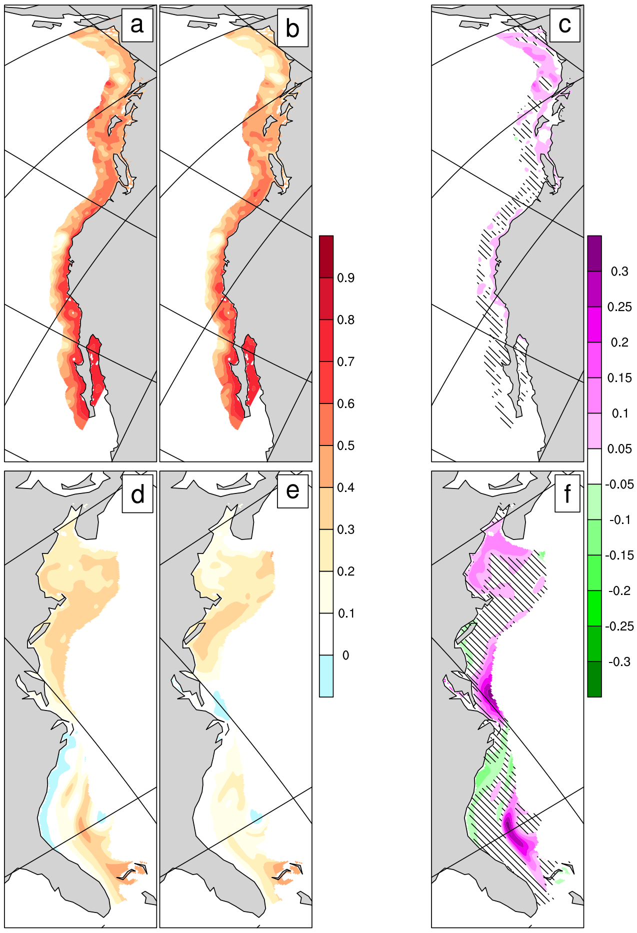

Figure 3. Anomaly correlation for Lead-7 month of (a,d) the downscaled hindcast and (b,e) the interpolated hindcast, verified against SSH anomaly from GLORYS reanalysis; (c,f) are the correlation difference between downscaling and interpolation; the hatching indicates the difference is not statistically significant at 0.1 level.

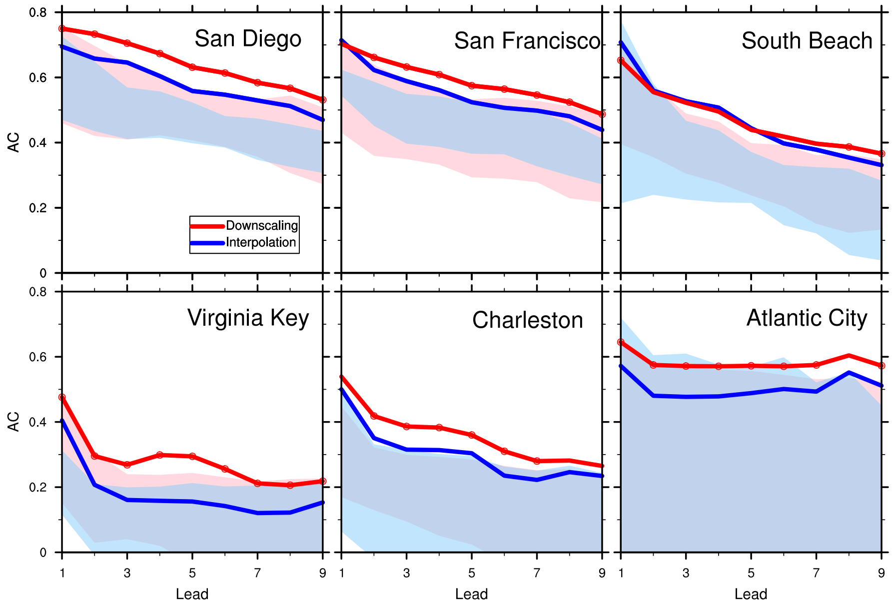

Figure 4. Anomaly correlation of the downscaled (red) and interpolated (blue) hindcast, verified against the tide gauge observation. The solid lines are the anomaly correlation of the respective ensemble mean of 6 models, and the shading indicates the skill range of all 6 models. The red circles indicate that the difference of the anomaly correlation between downscaling and interpolation is statistically significant at that lead time at 0.1 level.

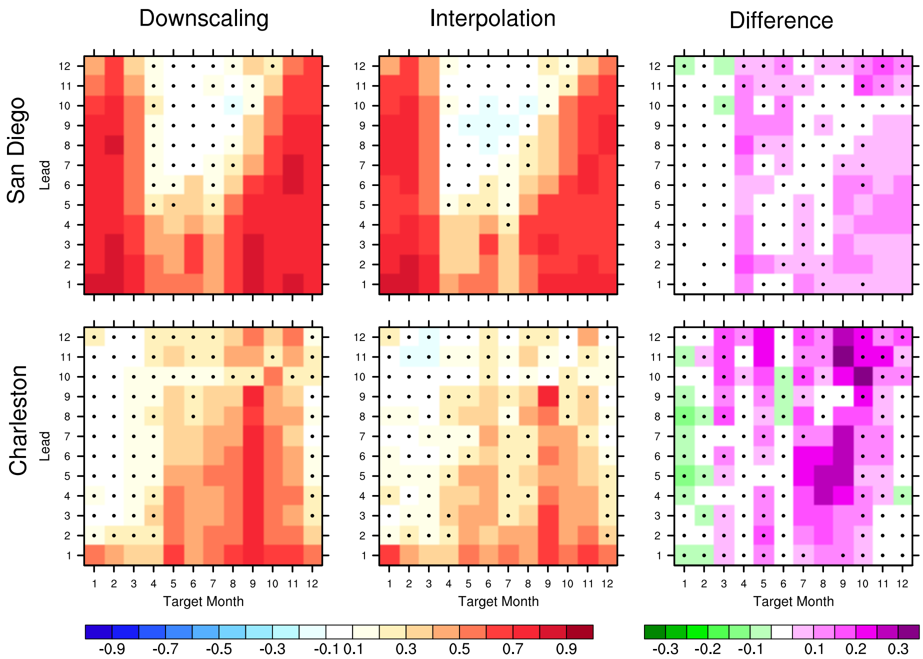

Figure 5. The Anomaly Correlation of the ensemble mean of downscaling (left column) and interpolation (middle column) of the hindcast, verified against the tide gauge observation at San Diego and Charleston, for each lead time and target month; the right column shows the correlation difference of downscaling and interpolation of the hindcast (downscaling minus interpolation). The black dot indicates the correlation or correlation difference is not statistically significant at that lead time and target month at 0.1 level.

Geophysical Research Letters

Supporting Information for

Statistical Downscaling of Seasonal Forecast of Sea Level Anomalies for US Coasts

Xiaoyu Long[1,2], Sang-Ik Shin[1,2] and Matthew Newman[1,2]

[1]CIRES, University of Colorado Boulder, Boulder, CO, USA
[2]NOAA Physical Sciences Laboratory, Boulder, CO, USA

Contents of this file

Text S1: Optimal Truncation

Since we built the linear regression in EOF space, we examined its sensitivity to the number of EOFs retained for each field in the regression, evaluating how EOF truncation impacted the downscaling operator's ability to reproduce the fine-scale GLORYS data from the coarse-grained GLORYS data. The downscaling was calculated using a 10-fold cross-validation, where 90% of the data was used to determine the operator, which was then used to downscale the remaining 10%; this process was cycled through ten times. As a metric of the goodness of fit for the resulting downscaled data, we computed the correlation between the downscaled fine-scale SSH anomalies and the original fine-scale SSH anomalies, evaluated along both time and spatial dimensions. Fig. S2a and d show this metric as a function of both predictor and predictand EOF truncation. For the West Coast, the best fit occurred with 34 /10 EOFs retained for the predictor/predictand. Additional EOFs eventually degrades the accuracy of the downscaling. For the East Coast, the best fit occurred for predictor/predictand truncation of 40/5 EOFs.

Text S2: SVD of the downscaling operator

What the downscaling operator (regression matrix) does is mapping the predictor space to the predictand space. SVD (singular vector decomposition) of the downscaling operator will help us better understand what modes in the predictor and predictand spaces contribute most to the downscaling.

The SVD of the downscaling operator is done as follows:

$$\mathbf{y} = \mathbf{B}\mathbf{x}$$
$$\mathbf{B} = \mathbf{U}\mathbf{\Sigma}\mathbf{V}^{\mathbf{T}}$$
$$\mathbf{y} = \mathbf{U}\mathbf{\Sigma}\mathbf{V}^{\mathbf{T}}\mathbf{x}$$

The column vectors in U constitute an orthonormal basis that spans the space of y, and the column vectors in V span the space of x. $\mathbf{\Sigma}$ is a diagonal matrix and its diagonal values are the singular values of the SVD of $\mathbf{B}$. In principle, the downscaling operator projects the predictor x onto each of the singular vector in V, then weights the projection by corresponding singular value, and finally multiplies by the singular vector in U. The relative magnitude of the singular vectors in V and the singular vector in U weighted by corresponding singular values indicates the pattern that has been amplified or damped in the downscaling process.

The dominant three singular vector pairs for each downscaling operator are shown in Fig. S4-5. Note that the relative magnitude difference between the left and right singular vectors indicates whether this specific structure was amplified or damped by the downscaling operator. For the west coast, the first singular vector pair (top row in Fig. S5) shows a pattern with the same sign all along the coast that is amplified by the downscaling, and likewise dominates the downscaling skill improvement (see Fig. S6). The second singular vector pairs is a dipole-like pattern also confined to the coast, amplified primarily in the Southwest coast. These patterns presumably represent effects of different phases of coastal Kelvin waves. The third singular vector pair has large magnitude off the coast, but the downscaling operator slight damps the pattern along the coast especially at the coast. The first and second singular pairs for the east coast are similar to that of the west coast, with the first one being a coherent structure and the second one being a dipole-like structure (Fig. S5). Note that the changing sign of the anomalies when moving from the coast to the offshore region indicates the influence of the strength of the boundary current on the coastal sea level variability through geostrophic balance.

In addition, to assess the importance of each singular vector pair in the downscaling, we reconstructed the downscaling operator **B** using different SV truncations. Then the different downscaling operator **B** was used to downscale the hindcast and the skill of the downscaled hindcast are accessed.

The skills of the downscaled hindcast using different truncation of the singular vectors (SVs) in Fig. S4-5 are shown in Fig. S6. For the west coast, the first SV pair is the most important while the skill is gradually improved by adding more SV pairs in the downscaling operator, with the exception for San Francisco. For the Virginia Key and Charleston, only the first pair of the SVs matters for the skill, and the skill degrades if adding more SVs in the downscaling operator. For Atlantic City, adding more SVs slightly improves the skill, but it is presumably due to the trend component in the dataset (not shown).

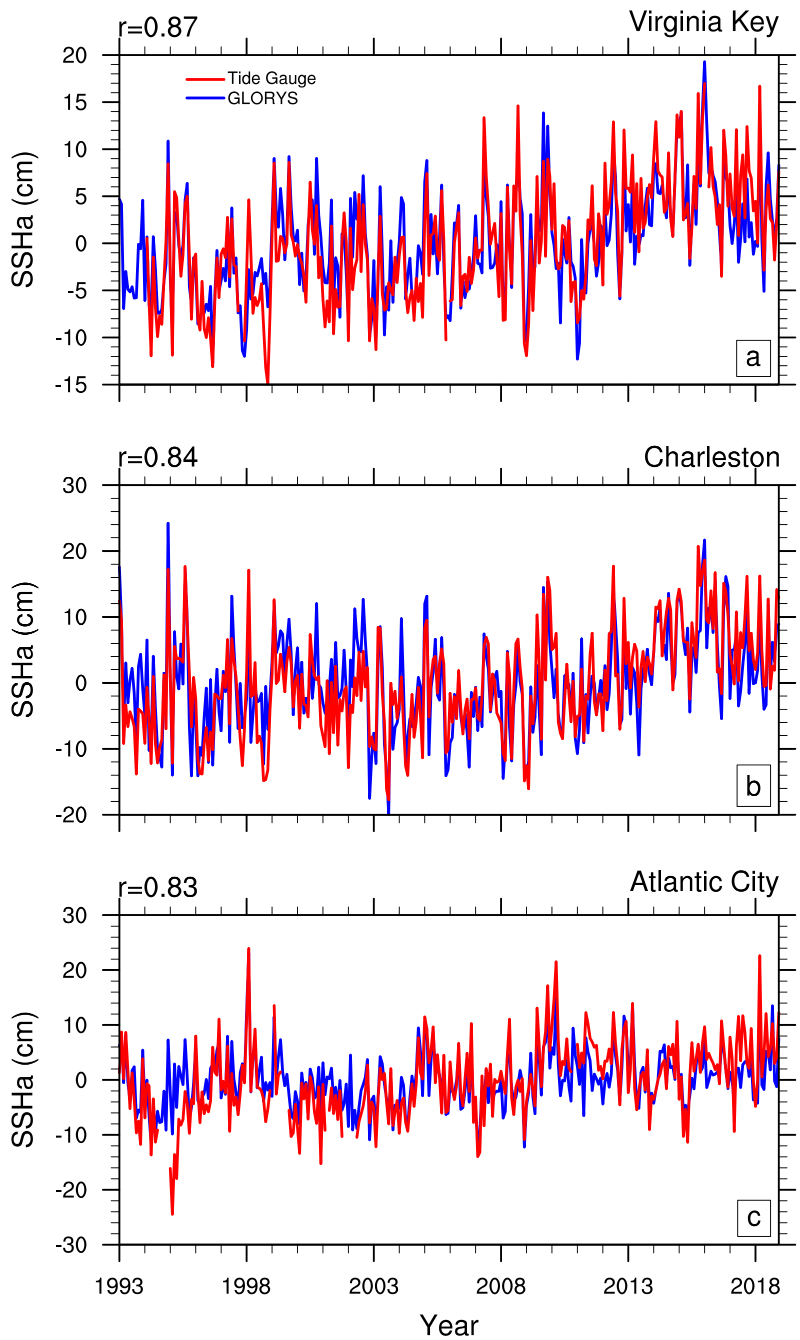

Fig. S1 The sea level anomalies for (a) Virginia Key, (b) Charleston and (c) Atlantic City, from GLORYS (blue) and tide gauge observation (red). The correlation coefficient between tide gauge observation and GLORYS for each station is shown on top of each panel. The nearest grid point in the GLORYS grids to each the tide gauge location is used. The unit is centimeter.

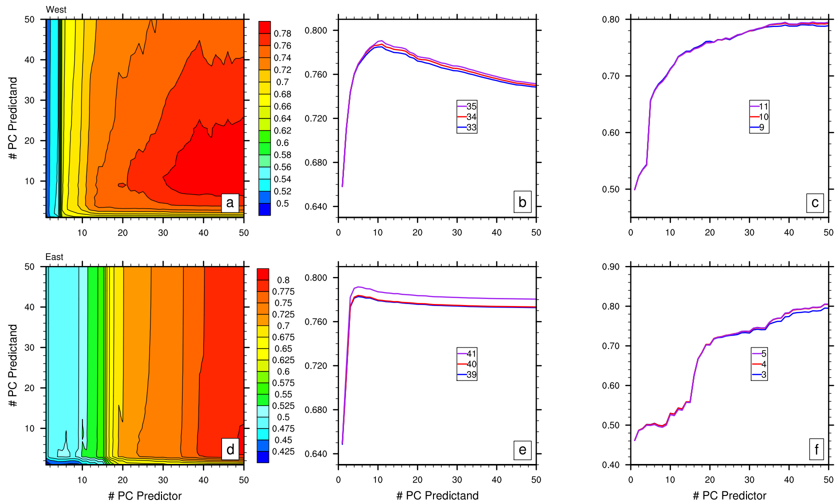

Figure S2. Space and time aggregated correlation coefficient between the SSH anomalies from GLORYS reanalysis and the observational downscaled SSH anomalies for (a,b,c) West Coast and (d,e,f) East Coast. (a,d) show the correlation coefficient as a function of the EOF truncation for predictor and predictand; and (b,c,e,f) show the correlation coefficient as a function of the EOF truncation for the predictor (predictand) with the predictand (predictor) fixed.

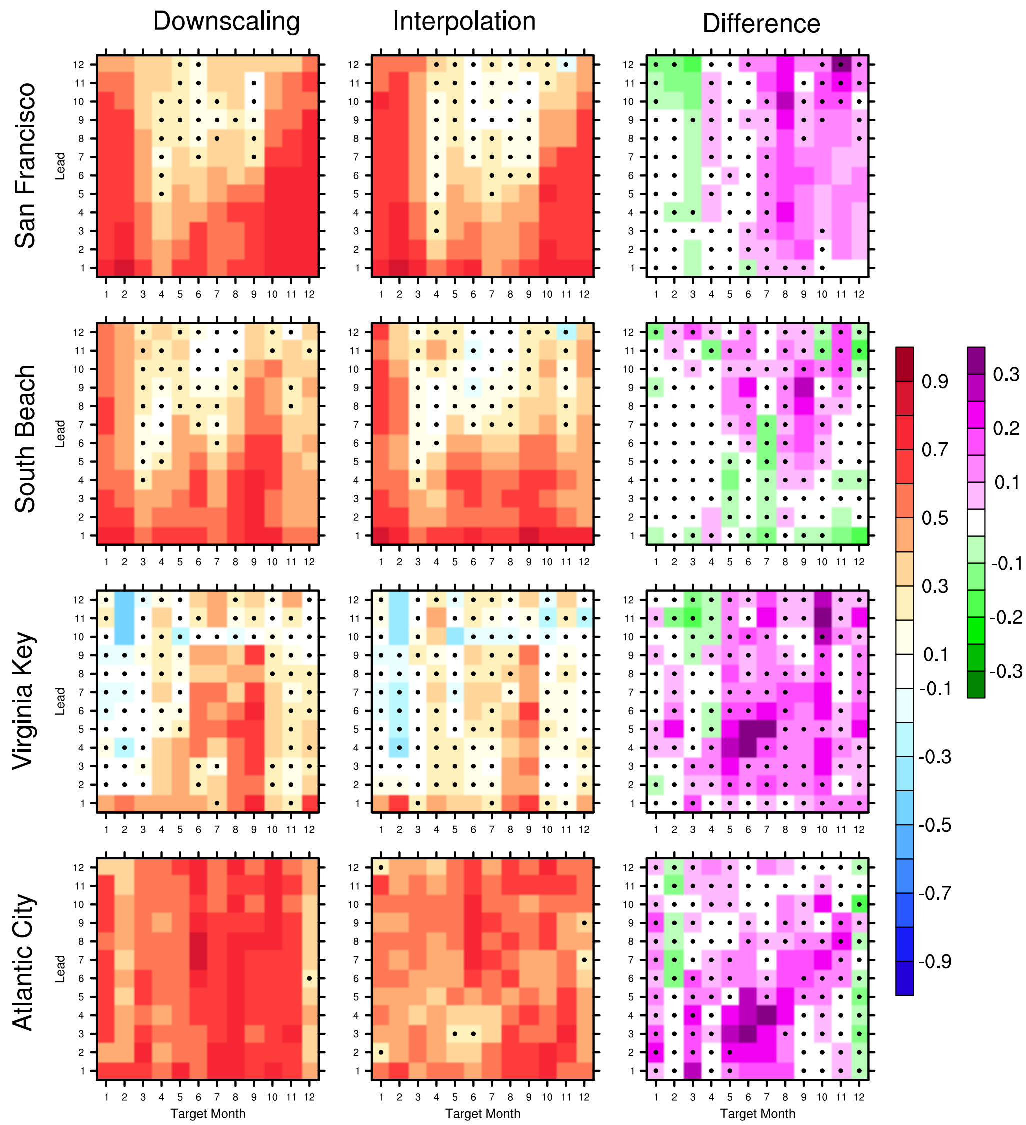

Figure S3. The Anomaly Correlation of the ensemble mean of downscaling (left column) and interpolation (middle column) of the hindcast, verified against the tide gauge observation at San Francisco, South Beach, Virginia Key and Atlantic City, for each lead time and target month; the right column shows the AC difference of downscaling and interpolation of the hindcast (downscaling minus interpolation). The black dot indicates the correlation or correlation difference is not statistically significant at 0.1 level at that lead time and target month.

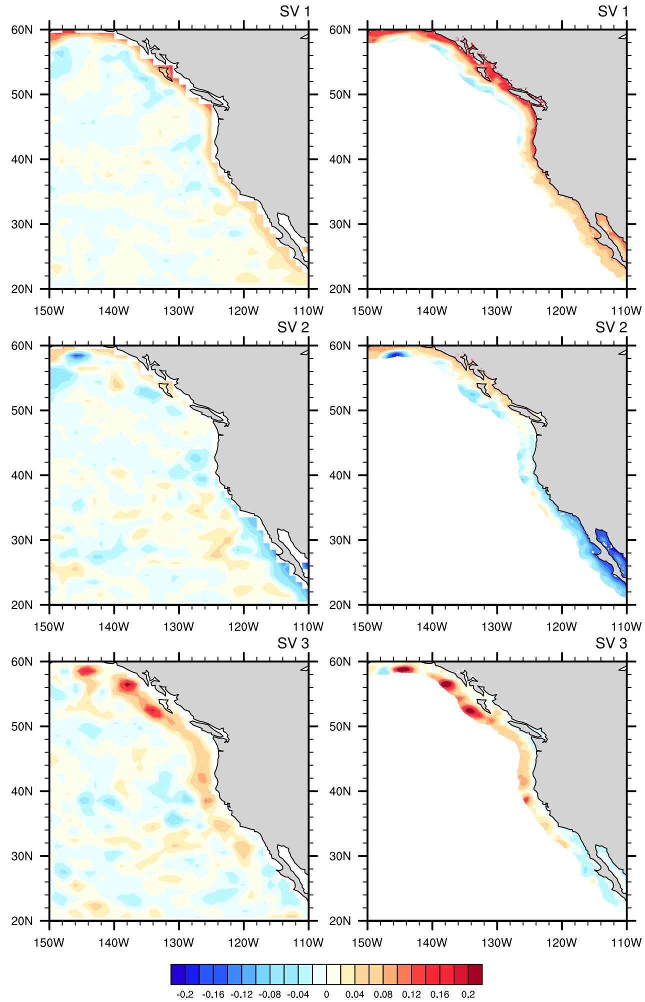

Fig. S4 The first three singular vector pairs from SVD of the regression matrix of the downscaling for the West Coast. Left column corresponds to the singular vectors related to predictor, and right column corresponds to the singular vectors related to predictor. The right column was weighted by the corresponding singular values so that the relative magnitude change from left column to right column represents the amplification from the regression matrix. The regression matrix is in EOF space, and the singular vector are reconstructed using the respective EOF patterns from reanalysis. The units of the singular vectors are arbitrary.

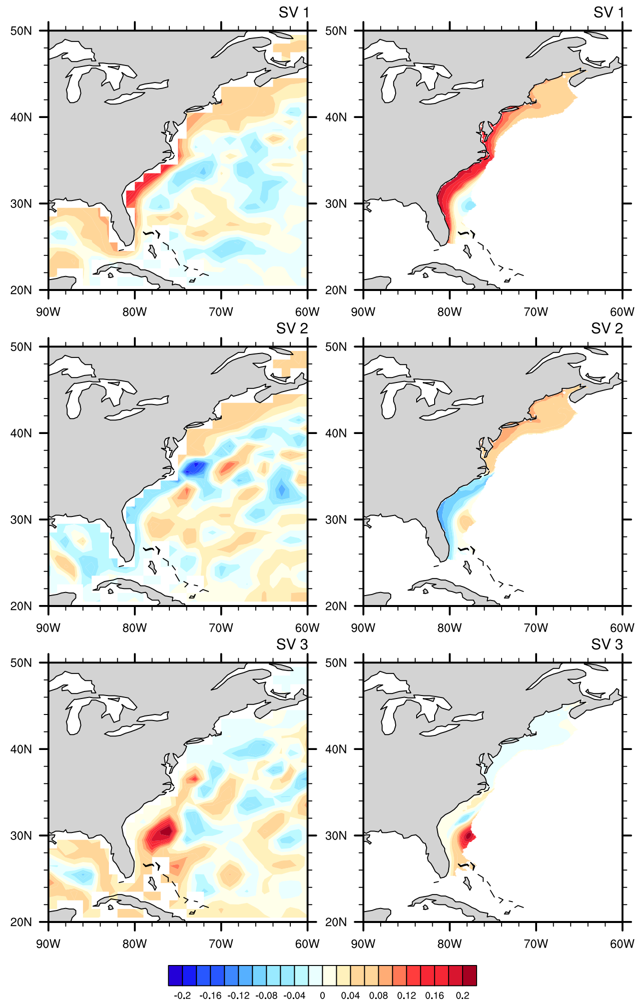

Fig. S5 Same as Figure S5 but for the East Coast.

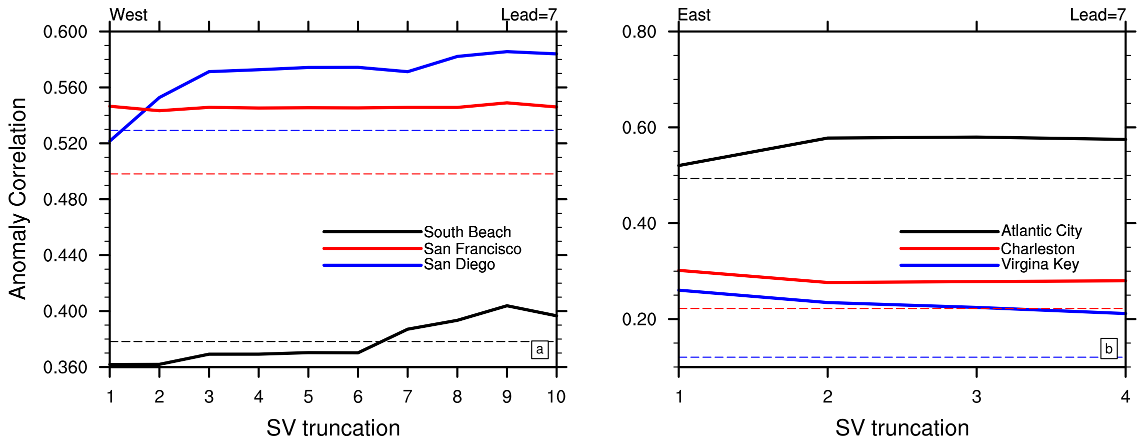

Fig. S6 The anomaly correlation between the downscaled hindcast (solid lines) or interpolated hindcast (dash lines) and the tide gauge observation for three tide gauge stations at (a) west coast and (b) east coast. The downscaled hindcast is constructed using different truncation of the singular vectors in the SVD of the regression matrix (see details in Text S1).

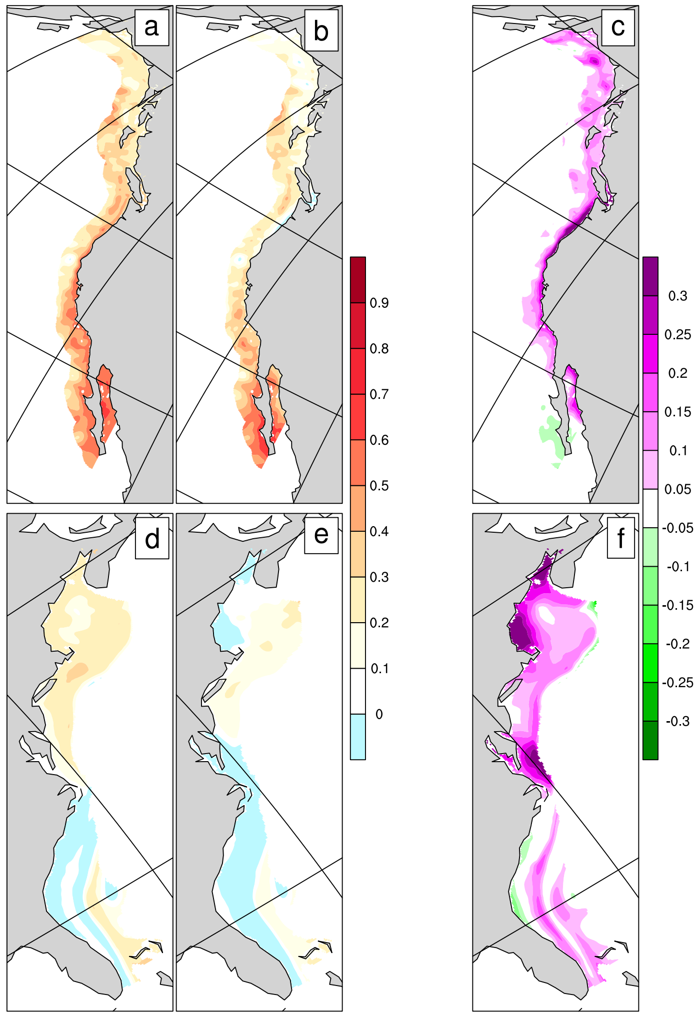

Fig. S7 Anomaly correlation for Lead-7 month of (a,d) the downscaled hindcast and (b,e) the interpolated hindcast from CanCM3, verified against SSH anomaly from GLORYS reanalysis; (c,f) are the correlation difference between downscaling and interpolation.

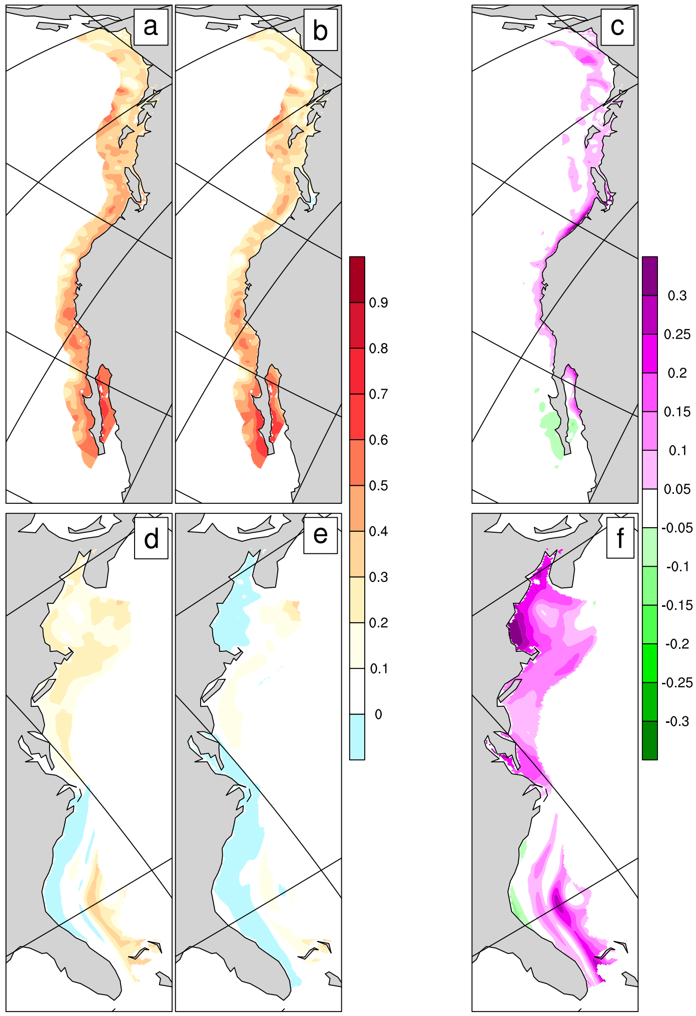

Fig. S8 Same as Fig S7 but for CanCM4 model.

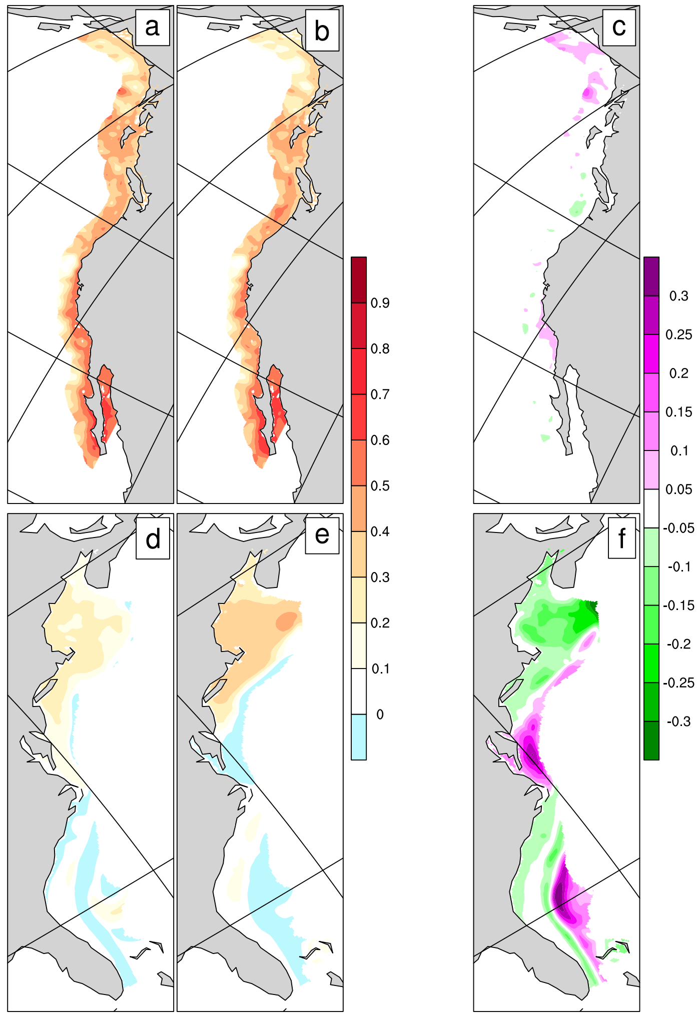

Fig. S9 Same as Fig. S7 but for CCSM4-UM model.

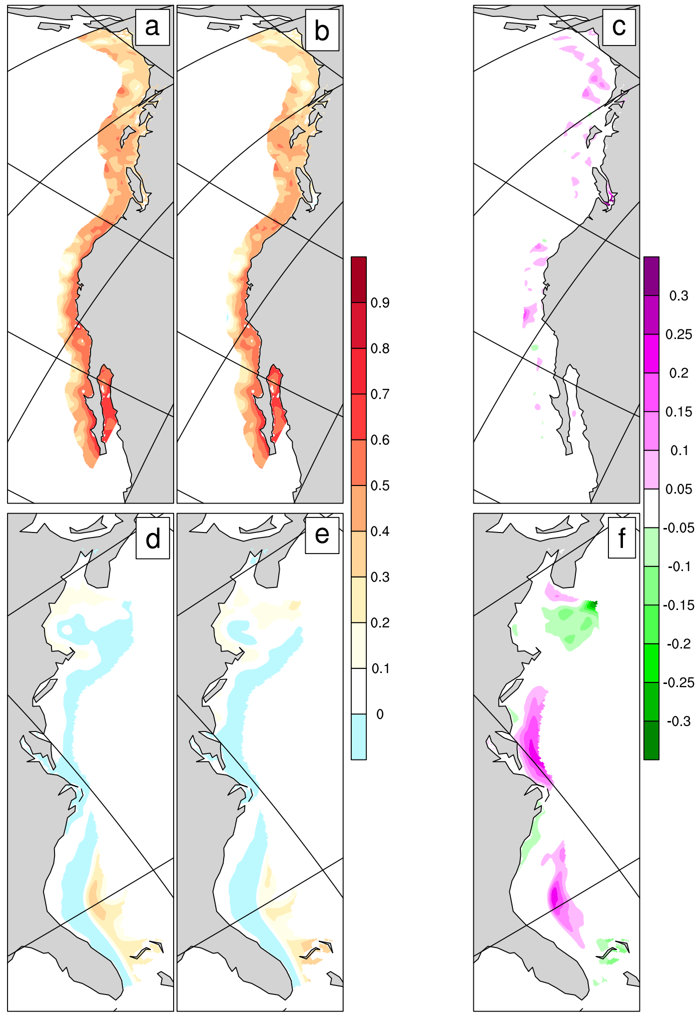

Fig. S10 Same as Fig. S7 but for CFSv2 model.

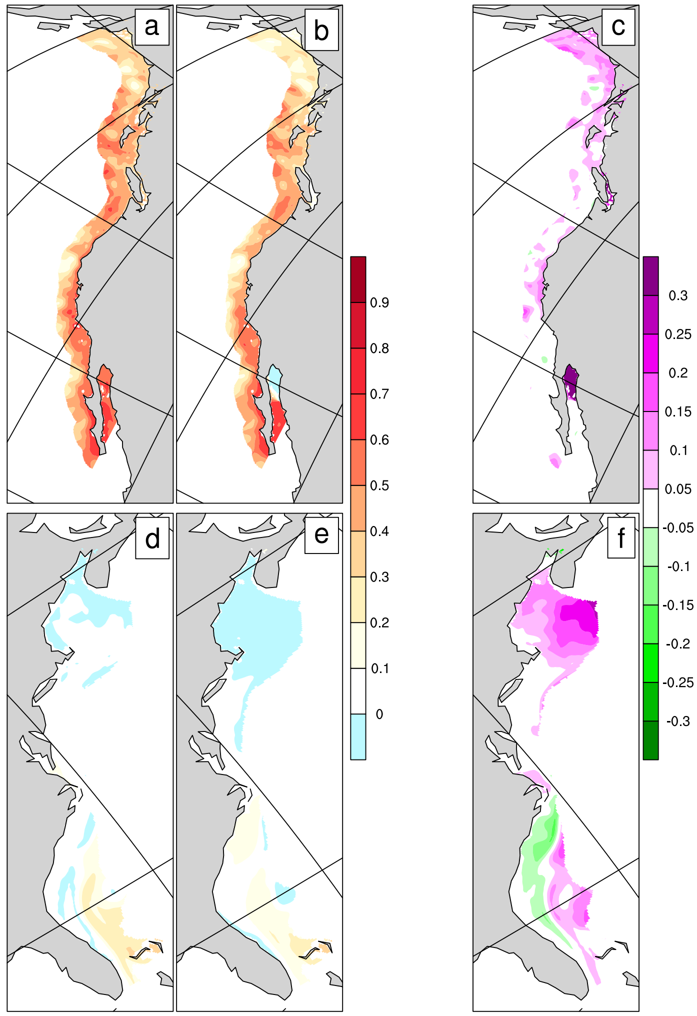

Fig. S11 Same as Fig. S7 but for GFDL model.

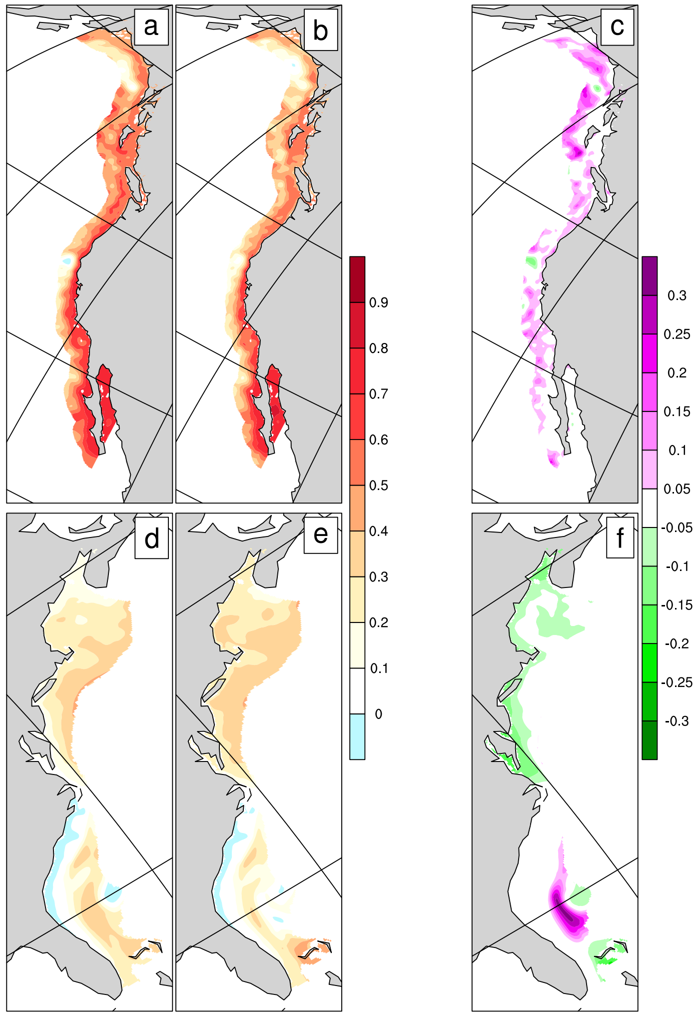

Fig. S12 Same as Fig. S7 but for ACCESS-S2 model.

Model	Organization	Ensemble size	Lead times	Resolution	Reference
(1) ACCESS-S2	Australian Bureau of Meteorology	12	1-9	0.25°	
(2) CanCM3	Canadian Meteorological Centre	10	1-12	1°	Merryfield et al. (2013)
(3) CanCM4	Canadian Meteorological Centre	10	1-12	1°	Merryfield et al. (2013)
(4) CCSM4-UM	University of Miami	10	1-12	1°	Kirtman et al. (2014)
(5) CFSv2	National Centers for Environmental Prediction	24 (28)	1-10	0.5°	Saha et al. (2014)
(6) GFDL CM2.1	Geophysical Fluid Dynamics Laboratory	10	1-12	1°	Zhang et al. (2007)

Table S1. Description of the 6 retrospective forecast systems used in this study. For each model system, the corresponding organization, ensemble size, maximum lead (months), nominal horizontal resolution of the ocean component (degrees), and a reference are indicated.